



Master's Thesis

Master in Telecommunication Engineering

Decomposition and unsupervised segmentation of
dual-polarized polarimetric SAR data using fuzzy
entropy and coherency clustering method

Ana Olivé Heras

Supervisor: Marc Bara Iniesta

Department of Telecommunications and Systems Engineering

**Escola Tècnica Superior d'Enginyeria (ETSE)
Universitat Autònoma de Barcelona (UAB)**

January 2015

El sotasignant, Marc Bara Iniesta, Professor de l'Escola Tècnica Superior d'Enginyeria (ETSE) de la Universitat Autònoma de Barcelona (UAB),

CERTIFICA:

Que el projecte presentat en aquesta memòria de Treball Final de Master ha estat realitzat sota la seva direcció per l'alumne Ana Olivé Heras.

I, perquè consti a tots els efectes, signa el present certificat.

Bellaterra, 20 de gener del 2015.



Signatura: Marc Bara Iniesta

Resum:

En aquesta tesi, el teorema de descomposició H- α i l'algorisme de segmentació fuzzy c-means s'apliquen a un conjunt de dades polarimètriques amb polarització dual d'un sistema SAR (Synthetic Aperture Radar) usant MATLAB i s'avalua la precisió de la segmentació. La segmentació es realitza amb l'objectiu de separar els diferents elements del paisatge emprant les característiques pròpies de cada mecanisme de dispersió. Com es veurà, els paràmetres d'entropia i d' α resulten molt valuosos per a diferenciar els diversos tipus d'objectius i l'algorisme fuzzy c-means proposat aplicat a l'entropia i a la matriu de coherència obté resultats robustos en el procés de segmentació. Ambdós algorismes s'apliquen sobre un conjunt de dades de Pangkalan Bun, Indonèsia, proporcionat pel satèl·lit radar TerraSAR-X.

Resumen:

En esta tesis, el teorema de descomposición H- α y el algoritmo de segmentación fuzzy c-means se aplican a un conjunto de datos polarimétricos con polarización dual de un sistema SAR (Synthetic Aperture Radar) usando MATLAB y se evalúa la precisión de la segmentación. La segmentación separa los diferentes elementos del paisaje usando las características propias de cada mecanismo de dispersión. Como se verá, los parámetros de entropía y de α resultan muy valiosos para diferenciar los tipos de objetivos y el algoritmo fuzzy c-means propuesto aplicado a la entropía y a la matriz de coherencia proporciona resultados robustos en la segmentación. Ambos algoritmos se aplican sobre un conjunto de datos de Pangkalan Bun, Indonesia, proporcionado por el satélite TerraSAR-X.

Summary:

In this thesis, H- α decomposition theorem and fuzzy c-means segmentation algorithm are applied to dual-polarized polarimetric SAR (Synthetic Aperture Radar) data using MATLAB and the accuracy of segmentation is evaluated. The segmentation is done with the purpose of separating the different elements of the landscape using the characteristics of the scattering mechanisms. As it will be shown, entropy and alpha decomposition parameters are a valuable key to differentiate between diverse types of targets and the proposed fuzzy c-means algorithm applied to the entropy and coherency matrix provides robust results in the segmentation process. Both algorithms are applied on a dual-polarized SAR dataset of Pangkalan Bun, Indonesia, provided by TerraSAR-X radar Earth observation satellite.

Table of Contents

1. Introduction	9
2. SAR fundamentals	11
2.1. Introduction to SAR	11
2.2. Geometry of SAR system	12
2.3. Range resolution	13
2.4. Azimuth resolution	14
2.5. Modes of operation	16
3. Polarimetric SAR analysis	18
3.1. Polarization state of electromagnetic waves	18
3.2. Polarization in SAR systems	20
3.3. Jones vector	22
3.4. Scattering or Sinclair matrix	23
3.5. Coherency matrix	25
4. Indonesia Case Study description	27
4.1. TerraSAR-X spacecraft	27
4.2. TerraSAR-X delivery file format	29
4.3. Description of the Indonesia dataset	30
5. H- α Decomposition applied to the Case Study	33
5.1. Theory of H- α Decomposition	33
5.1.1. Extraction of the H- α parameters	34
5.1.2. Interpretation of H- α feature space	35
5.2. Application of H- α Decomposition to the Case Study	37
5.3. Decomposition results of the Case Study	37

6. Fuzzy clustering applied to the Case Study	46
6.1. Theory of Fuzzy clustering	46
6.1.1. Fuzzy partition	47
6.1.2. Fuzzy c-Means Functional	48
6.1.3. Fuzzy c-Means Algorithm	49
6.2. Application of Fuzzy clustering to the Case Study	50
6.3. Segmentation results of the Case Study	51
7. Conclusions	58
References	60

List of Tables

Table 1.	Jones vectors and the corresponding polarization ellipse parameters for some canonical polarization states	23
Table 2.	Main parameters of TerraSAR-X satellite	27
Table 3.	Processing levels of TerraSAR-X satellite	29
Table 4.	Characteristics of the TerraSAR-X Indonesia dataset	30
Table 5.	Zones of H- α feature space	36

List of Figures

Fig. 1.	Side-looking geometry of a monostatic SAR system	12
Fig. 2.	Geometric representation of slant range and ground range resolution Azimuth resolution	13
Fig. 3.	Geometric representation of azimuth resolution	14
Fig. 4.	Stripmap mode	16
Fig. 5.	Spotlight mode	16
Fig. 6.	ScanSAR mode	17
Fig. 7.	Electric field of linear or plane polarization	18
Fig. 8.	Electric field of circular polarization	19
Fig. 9.	Polarization ellipse	20
Fig. 10.	Artist view of TerraSAR-X satellite	28
Fig. 11.	Map of the area covered by the Case Study dataset	30
Fig. 12.	Reconstruction image of the entire dataset and HH channels of the three selected subsets	31
Fig. 13.	Aerial image of the three subsets captured by Google Earth and their corresponding HH channel matrix image	32
Fig. 14.	H- α classification plane	35
Fig. 15.	Overall data flow diagram for the Case Study	37
Fig. 16.	Polarimetric channels of the subset A: (a) HH-channel, (b) VV-channel	37
Fig. 17.	Polarimetric channels of the subset A with 5x5 multilook window: (a) HH-channel, (b) VV-channel	38
Fig. 18.	Parameters extracted from the subset A: (a) entropy, (b) alpha angle	39
Fig. 19.	Zoom of the zones with the highest alpha in subset A produced by the yellow buildings	40
Fig. 20.	H- α plane of the subset A: (a) zones with different colors, (b) density plot of the plane	40
Fig. 21.	Subset A classified using H- α plane: (a) subset A, (b) area of subset A in detail	41
Fig. 22.	Parameters extracted from the subset B: (a) entropy, (b) alpha angle	41

Fig. 23.	H- α plane of the subset B: (a) zones with diferent colors, (b) density plot of the plane	42
Fig. 24.	Subset B classified using H- α plane	43
Fig. 25.	Parameters extracted from the subset C: (a) entropy, (b) alpha angle	43
Fig. 26.	H- α plane of the subset C: (a) zones with diferent colors, (b) density plot of the plane	44
Fig. 27.	Subset C classified using H- α plane: (a) subset C, (b) area of subset C in detail	44
Fig. 28.	Objective function values in the first 50 iterations for the subset A	51
Fig. 29.	Segmented and pseudo-colored image of the subset A after applying the fuzzy c-means algorithm: (a) after 5 iterations, (b) after 10 iterations, (c) after 25 iterations and (d) after 50 iterations	52
Fig. 30.	Different classes obtained in the three-dimensional space after applying the fuzzy c-means algorithm in the subset A	53
Fig. 31.	Objective function values in the first 50 iterations for the subset B	53
Fig. 32.	Segmented and pseudo-colored image of the subset B after applying the fuzzy c-means algorithm: (a) after 5 iterations, (b) after 10 iterations, (c) after 25 iterations and (d) after 50 iterations	54
Fig. 33.	Different classes obtained in the three-dimensional space after applying the fuzzy c-means algorithm in the subset B	55
Fig. 34.	Objective function values in the first 50 iterations for the subset C	56
Fig. 35.	Segmented and pseudo-colored image of the subset C after applying the fuzzy c-means algorithm: (a) after 5 iterations, (b) after 10 iterations, (c) after 25 iterations and (d) after 50 iterations	56
Fig. 36.	Different classes obtained in the three-dimensional space after applying the fuzzy c-means algorithm in the subset C	57

Chapter 1

Introduction

Synthetic Aperture Radar (SAR) is nowadays one of the most important devices used in remote sensing for Earth observation. Lake and river ice monitoring, cartography, crop production forecasting and coastal surveillance are some of the applications in which SAR is particularly useful due to the strong advantages that offers over optical satellite imagery [1]. These advantages range from being able to operate in 24-hour all-weather conditions to acquiring broad-area imaging at high resolutions, which can be really costly in traditional radar imagery.

SAR polarimetry has become increasingly popular in recent years. Single-polarization SAR systems use a single linear polarization; transmitting and receiving horizontally or vertically polarized radiation. Current satellite SAR missions are capable of delivering polarimetric imagery, which provides a more complete description of the target scattering behavior than traditional single-channel SAR data [2]. Hence, multi-polarization imagery is more appropriate for target recognition and land use segmentation since it is more sensitive to the properties of the ground objects and produces more accurate classification results. Dual-polarization systems consider two linear polarizations; while full-polarization systems alternately transmit two orthogonal polarizations and record both received polarizations. Full-polarization systems are able to extract expanded information of the target, but they have a high operational cost and higher antenna transmitter power requirements. Therefore, dual-polarization SAR systems are commonly used instead; moreover, they provide a wider swath width and greater area coverage compared to full-polarization systems, at expenses of losing some target scattering properties.

The physical and mathematical information of scattering media from the radar measurements is extracted using target decomposition theorems [3]. The ones based on the eigenvalue

decomposition of the coherency matrix, obtained from the data, have been revealed as the most suitable to perform data interpretation in the study and characterization of natural targets from polarimetric data. It is the case of H- α decomposition, a target decomposition theorem that extracts the entropy and alpha angle parameters to allow identifying the scattering mechanisms and the properties of the polarimetric data. Entropy demonstrates the randomness of the underlying scattering mechanisms and alpha angle is used to define the type of scattering mechanisms.

Image segmentation, whose objective is to divide the image into different meaningful regions with homogeneous characteristics, is a key step toward the SAR image analysis and classification. One of the existing segmentation techniques is clustering, which is currently being explored in polarimetric SAR images. Its purpose is to identify natural groupings of data from a large dataset, which results in concise representation of the behavior of the system. Fuzzy c-means clustering is the most wide spread clustering approach for image segmentation because of its robust characteristics for data classification.

In this work, an unsupervised segmentation for dual-polarized polarimetric SAR data is presented; as well as the intermediate steps of target decomposition, in this case H- α decomposition theorem is used, and image segmentation, using fuzzy c-means clustering by means of entropy and diagonal coherency matrix parameters. All the algorithms have been developed in MATLAB computer environment and the dataset used for testing is provided by TerraSAR-X radar Earth observation satellite.

Chapter 2

SAR fundamentals

2.1 Introduction to SAR

Synthetic Aperture Radar (SAR) is based on the generation of an effective long antenna by signal-processing means rather than by the use of a long physical antenna [4]. Only a single and relatively small physical antenna is used in most cases and this is enough to acquire high resolutions. SAR uses a single beam-forming antenna carried on a moving platform, which can be an aircraft or a satellite. The platform travels along a path transmitting microwave pulses towards the ground. Some of the transmitted microwave energy is reflected back towards the sensor where it is received as a signal. The received signal is first pre-processed, involving demodulation, to create the raw data and then is processed applying image formation algorithms to obtain a reflectivity map image. Hence, SAR obtains high resolutions simulating a real aperture by integrating the pulse echos into a composite signal. It is possible after applying appropriate processing to simulate effective antenna lengths up to 100 m or more [5].

Since SAR works in the microwave region of the electromagnetic spectrum, usually between P-band and Ka-band [6], it avoids weather-related limitations like cloud-cover or rainfall. So, it achieves equally good results in all weather conditions and also is independent of lighting conditions, acquiring accurate data at day or night.

In the last years, SAR technology has improved and the data collection has achieved high reliability and quality, so the demand for using SAR in a variety of applications is increasing. It has military applications and earth-science related applications such as mapping and

monitoring vegetation and sea-ice, terrain classification, finding minerals and evaluation of environmental damages, among others. Currently, the coverage rates of an airborne SAR system are capable of exceeding $1 \text{ km}^2/\text{s}$ at a resolution of 1 m^2 , thus producing over one million pixels each second [7].

2.2 Geometry of SAR system

The side-looking geometry of a monostatic SAR system is shown in Figure 1. The SAR sensor borne on a satellite platform flies over the territory that is sensed at a certain velocity, illuminating with pulses of electromagnetic radiation the Earth surface perpendicular to the flight line direction [8].

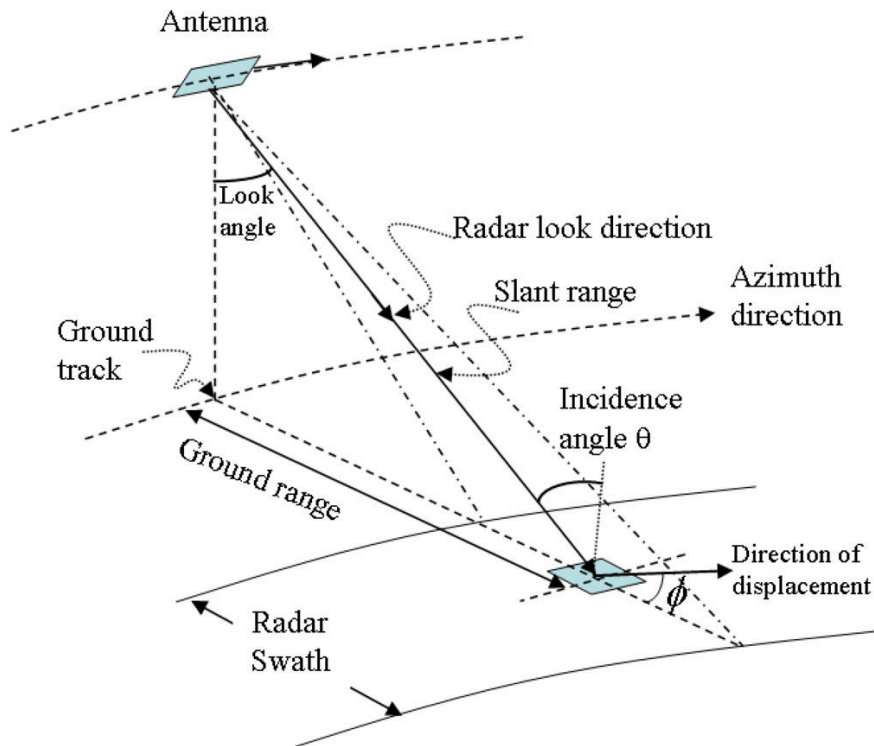


Fig. 1. Side-looking geometry of a monostatic SAR system

The direction of travel of the platform is referred to as the *azimuth* or *along-track* direction. The distance from the sensor to the ground is the *slant range*. *Ground range* refers to the across-track dimension perpendicular to the flight direction [9]. The angle from which the satellite observes the surface is the *look angle*. The *incidence angle* θ relates the direction of the radar pulses towards the normal vector of the terrain. The incidence angle is commonly used to describe the angular relationship between the radar beam and the ground, surface layer or a target [10].

The antenna beam of a side-looking radar is directed perpendicular to the flight path and illuminates a swath parallel to the platform ground track. The *radar swath* is the width of the imaged scene in the range dimension, so it refers to the strip of the Earth's surface from which data are collected by the radar. The portion of the image swath closest to the nadir track of the radar platform is called the *near range* while the portion of the swath farthest from the nadir is called the *far range* [11].

2.3 Range resolution

Range resolution is the ability of the radar system to distinguish between two or more targets on the same bearing but at different ranges [12]. Pulse width is the primary factor in range resolution. For a single frequency waveform, short pulses mean a fine range resolution but at the same time it is important that these short pulses have high energy to enable the detection of the reflected signals in order to obtain a good value of signal-to-noise ratio (SNR). This is accomplished by using pulse compression techniques. These techniques consist of emitting pulses that are linearly modulated in frequency for a duration of time T_p [13]. The frequency of the signal, called *chirp*, sweeps a band B and it is centered on a carrier at frequency f_0 . The received signal is then processed with a matched filter that compresses the long pulse to an effective duration equal to $1/B$. Range resolution is also dependent of the look angle but independent of the height of the antenna to the surface.

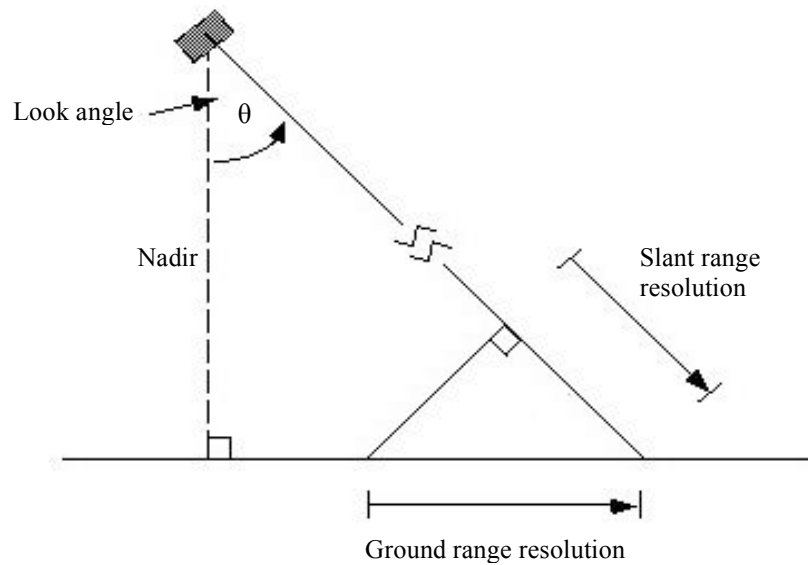


Fig. 2. Geometric representation of slant range and ground range resolution

The ground range resolution δx is the change in ground range associated with a slant range resolution of δr and is given by (1).

$$\delta x = \frac{\delta r}{\sin \theta} \quad (1)$$

where θ is the incidence angle and δr is given by (2).

$$\delta r = \frac{c}{2B} \quad (2)$$

where c is the speed of light and $1/B$ is the effective duration of the pulse. Hence, according to the formulas, a well-designed radar system with maximum efficiency should be able to distinguish targets separated by one-half the pulse width time. This way the echoes received do not overlap.

2.4 Azimuth resolution

Azimuth resolution is the minimum distance on the ground in the direction parallel to the flight path of the aircraft at which two targets can be separately imaged [4]. Azimuth resolution is dependent on aperture length and radar wavelength. The longitude of a SAR antenna is synthesized corresponding to the amount of time that the target remains illuminated while the sensor is flying overhead. This way the resolution of the azimuth direction is improved since a large antenna aperture is simulated.

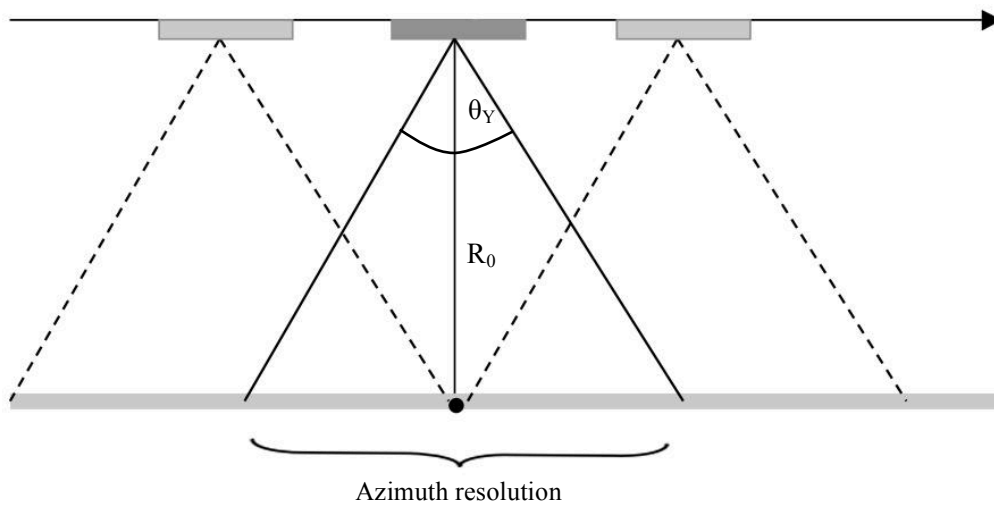


Fig. 3. Geometric representation of azimuth resolution

Two targets in the azimuth or along-track resolution can be separated only if the distance between them is larger than the radar beamwidth [14], so they cannot be in the radar beam at the same time.

The azimuth resolution for a real antenna with a beam width θ_Y at range R_0 is given by (3).

$$\delta y = R_0 \theta_Y \quad (3)$$

Taking into account that the antenna beam width is proportional to the aperture size [15],

$$\theta_Y \approx \frac{\lambda}{L_Y} \quad (4)$$

where L_Y refers to the physical dimensions of the real antenna aperture along the azimuth direction and λ is the wavelength corresponding to the carrier frequency of the transmitted signal. So, the azimuth resolution results in (5).

$$\delta y = \frac{R_0 \lambda}{L_Y} \quad (5)$$

It is observed, according to the formula, that high resolution in azimuth requires large antennas. In order to achieve high resolution the concept of synthetic aperture is applied. The resulting synthetic beam width is (6) [16].

$$\theta_Y = \frac{L_Y}{2 \cdot R_0} \quad (6)$$

So, the corresponding azimuth resolution for a synthetic aperture antenna when the scatterer is coherently integrated along the flight track results in (7).

$$\delta y = \frac{L_Y}{2} \quad (7)$$

It is observed that the azimuth resolution is dependent only of the physical size of the real antenna and independent of the range or wavelength.

2.5 Modes of operation

In SAR operations there are generally three imaging modes for data collection; they are stripmap mode, spotlight mode and scanSAR mode [17].

- Stripmap mode:

In this mode the ground swath is illuminated with a continuous sequence of pulses while the antenna pointing is fixed in elevation and azimuth relative to the flight line (usually normal to the flight line) [18]. The data acquired is an image strip with continuous image quality in azimuth and follows the length contour of the flight line of the platform itself. This mode is usually used for the mapping of large areas of terrain.

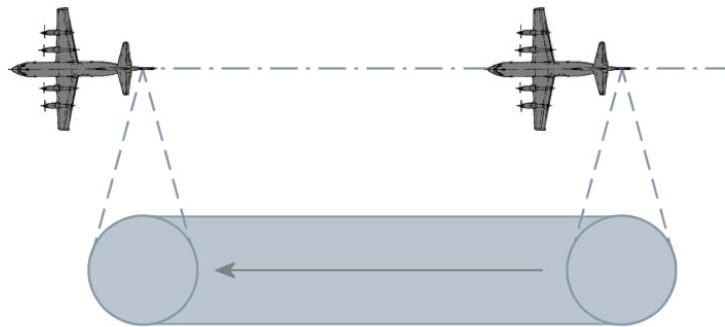


Fig. 4. Stripmap mode

- Spotlight mode:

During the observation of a particular ground scene the radar beam is steered so that the predetermined area of interest is continuously illuminated while the aircraft flies by in a straight line; hence the synthetic aperture becomes larger [19].

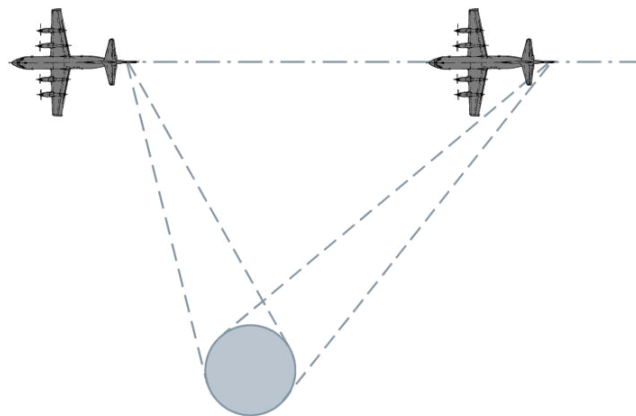


Fig. 5. Spotlight mode

This mode is capable of extending the high-resolution SAR imaging capability significantly since when more pulses are used, the azimuth resolution is increased. In spotlight mode the spatial coverage is reduced, since other areas within a given accessibility swath of the SAR cannot be illuminated while the radar beam is spotlighting over a particular target area.

- ScanSAR mode:

This mode achieves a wider imaged swath by scanning several adjacent ground sub-swaths with simultaneous beams, each with a different incidence angle [20]. ScanSAR mode provides large area coverage at the expense of azimuth resolution.

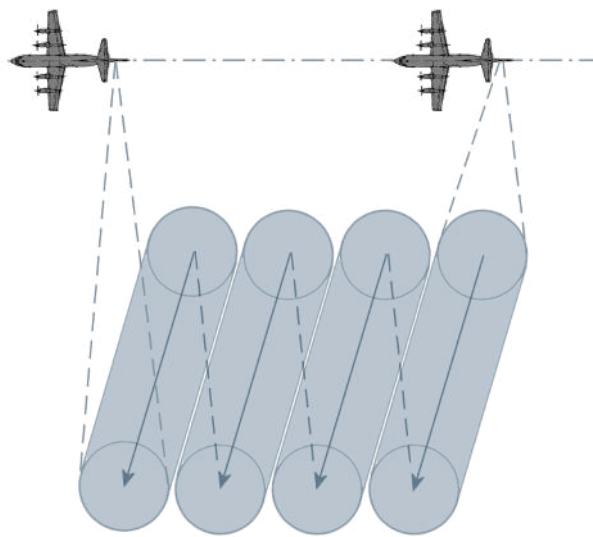


Fig. 6. ScanSAR mode

Chapter 3

Polarimetric SAR analysis

3.1 Polarization state of electromagnetic waves

Electromagnetic waves are formed when an electric field couples with a magnetic field. The magnetic and electric fields of an electromagnetic wave are perpendicular to each other and to the direction of the wave. For a plane electromagnetic wave, polarization refers to the locus of the electric field vector in the plane perpendicular to the direction of propagation [21]. The polarization is described by the geometric figure traced by the electric field vector upon a stationary plane perpendicular to the direction of propagation, as the wave travels through that plane [22].

Most of the polarized radars use two orthogonal linearly polarized antennas; hence the Cartesian coordinate system is used as in Figure 7.

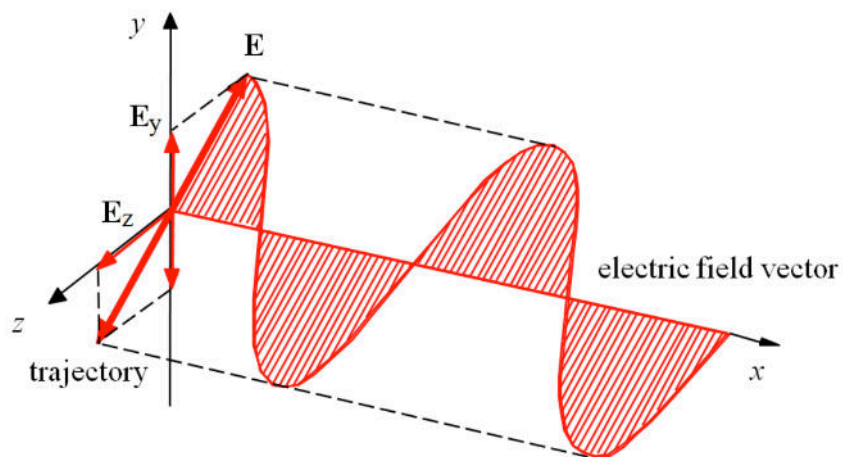


Fig. 7. Electric field of linear or plane polarization

In Figure 7, x indicates the direction of wave propagation and the corresponding electric field is located in y - z plane and E_y and E_z are the y -component and z -component of the electric field vector E respectively. The figure shows a linear polarization of an electromagnetic wave. If the oscillation of the electric field vector is observed from behind toward the propagation direction in x -axis, the trajectory becomes a line on y - z plane. The polarization is vertical when the electric lines of force lie in a vertical direction and is horizontal when the electric lines of force lie in a horizontal direction.

Electromagnetic wave propagation of circular polarization is illustrated in Figure 8. Circular polarization has the electric lines of force rotating through 360 degrees with every cycle of energy [23].

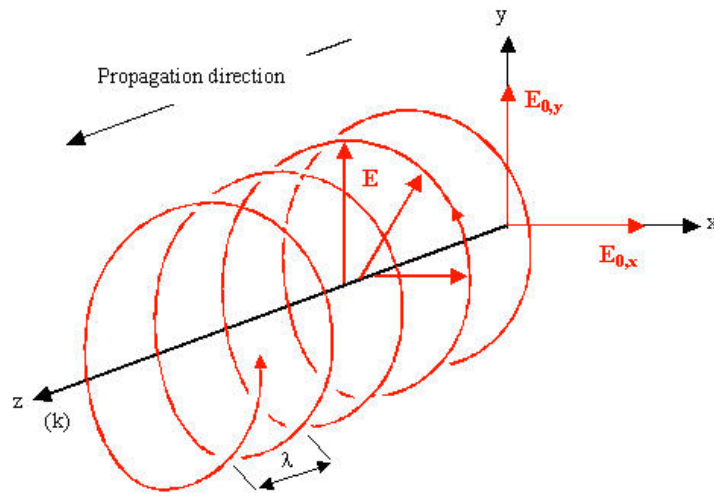


Fig. 8. Electric field of circular polarization

The amplitudes of the y -component and z -component of the electric field vector in circular polarization are the same but the phase between them is different. The oscillation direction rotates with time as the electric field propagates with constant amplitude. When looking at the source the electric vector of the wave appears to be rotating counterclockwise, it is called right hand circular polarization. If it appears rotating clockwise, then is the case of left hand circular polarization.

Elliptical polarization consists of two perpendicular electric field components of unequal amplitude and unequal phase [24]. The trace of elliptic polarization, as in circular polarization, rotates either in the left-hand direction or in the right-hand direction, depending on the phase difference. Figure 9 is called *polarization ellipse* and can be expressed in terms of two angular parameters: the orientation angle ψ ($0 \leq \psi \leq \pi$) and the eccentricity or ellipticity

angle χ ($-\pi/4 < \chi \leq \pi/4$) [25]. The angle ψ is the angle between z-axis and the major axis of the ellipse while the angle χ describes the degree to which the ellipse is oval.

The angle χ is given by (8).

$$\chi = \arctan\left(\frac{b}{a}\right) \quad (8)$$

where a is the length of the semi-major axis of the ellipse and b is the length of the semi-minor axis of the ellipse, as shown in Figure 9.

Linear and circular polarizations are special cases of elliptical polarization. If the major and minor axes of the ellipse are equal ($a = b$), then $\chi = -\pi/4, \pi/4$ and the elliptic polarization becomes the circular polarization. When $b = 0$, then $\chi = 0$ and the trace of the tip of the electric field will be a straight line and the elliptic polarization becomes the linear polarization, with an orientation of 45° .

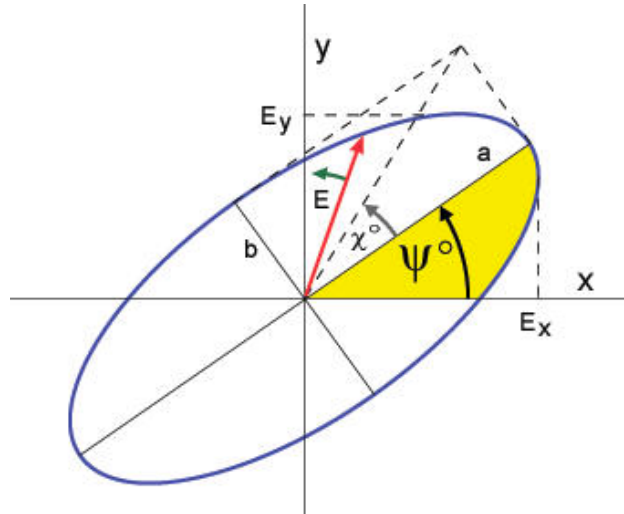


Fig. 9. Polarization ellipse

3.2 Polarization in SAR systems

The antennas of SAR systems are designed to transmit and receive electromagnetic waves of a specific polarization. To create a wave with an arbitrary polarization, it is necessary to have signals with components in two orthogonal or basis polarizations. The two most common basis polarizations in SAR are horizontal linear (H) and vertical linear (V). Circular polarization is used in some applications (for example in weather systems).

In the simpler SAR systems, the antenna is configured in order to use the same polarization in transmission and reception. This traditional kind of radar does not allow determining the complete vector nature of the scattered signal since there is a loss of information regarding the target or the target is completely missed by the radar if the scattered signals have orthogonal sense of polarization. In the more complex systems the antenna is usually designed to transmit and receive waves at more than one polarization (polarimetric radar), which facilitates the complete characterization of the scatterer [26]. A switch is used to direct energy to the different parts of the antenna in sequence, so waves of different polarizations can be transmitted separately (e.g. the H and V parts). Referring to the reception, the antenna is designed to be able to receive the different polarization components of the electromagnetic wave at the same time, because the scatterer can change the polarization of the scattered wave to be different from the incident wave polarization. Those changes in the polarization state of the scattered waves depend upon the characteristic features of the object (scatterer).

A pair of symbols is usually used to denote the transmission and reception polarizations of the system [27]. In the case of a SAR system that uses H and V linear polarizations, the possible channels are the following ones:

- HH: horizontal linear transmission and horizontal linear reception
- HV: horizontal linear transmission and vertical linear reception
- VH: vertical linear transmission and horizontal linear reception
- VV: vertical linear transmission and vertical linear reception

The polarization combinations that use the same polarization in transmission and in reception are called like-polarized (HH and VV). When the transmit and receive polarizations are orthogonal to one another (HV and VH), the combinations are called cross-polarized [28].

According the level of polarization complexity, the SAR system can be classified as [27]:

- Single-polarized: there is a single-polarization transmitted and a single-polarization received (HH or VV or HV or VH imagery).
- Dual-polarized: transmit a horizontally or vertically polarized waveform and measure signals in both polarizations in receive (HH and HV, VV and VH, or HH and VV imagery).

- Full-polarized or quad-polarized: alternate between transmitting H and V polarized waveforms and receive both H and V (HH, HV, VH and VV imagery).

SAR polarimetry extracts more detailed information of targets on land and sea than conventional single-polarized SAR imagery, from the combinations of transmitted and received signals of different polarization states. Polarimetric SAR data is useful for analyzing different scattering processes and for image classification.

3.3 Jones vector

The representation of a plane monochromatic electric field in the form of a Jones vector aims to describe the wave polarization using the minimum amount of information [6].

An electric field vector in an orthogonal basis $(\hat{x}, \hat{y}, \hat{z})$, located in the plane perpendicular to the direction of propagation along \hat{z} can be represented in time domain as (9).

$$\vec{E}(z, t) = \begin{bmatrix} E_{0x} \cos(\omega t - kz + \delta_x) \\ E_{0y} \cos(\omega t - kz + \delta_y) \end{bmatrix} = \text{Re} \left\{ \begin{bmatrix} E_{0x} e^{j\delta_x} \\ E_{0y} e^{j\delta_y} \end{bmatrix} e^{-jkz} e^{j\omega t} \right\} = \text{Re} \{ \underline{\vec{E}}(z) e^{j\omega t} \} \quad (9)$$

For the monochromatic case, the time dependence is neglected. A Jones vector \underline{E} is then defined from the complex electric field vector $\underline{\vec{E}}(z)$ as (10).

$$\underline{E} = \underline{\vec{E}}(z)|_{z=0} = \underline{\vec{E}}(0) = \begin{bmatrix} E_{0x} e^{j\delta_x} \\ E_{0y} e^{j\delta_y} \end{bmatrix} \quad (10)$$

The Jones vector completely defines the amplitude and phase of the complex orthogonal components (in x and y directions) of an electric field. A Jones vector can be formulated as a 2-D complex vector function of the polarization ellipse characteristics as (11) [6]

$$\underline{E} = A e^{j\alpha} \begin{bmatrix} \cos\psi \cos\chi - j \sin\psi \sin\chi \\ \sin\psi \cos\chi + j \cos\psi \sin\chi \end{bmatrix} = A e^{j\alpha} \begin{bmatrix} \cos\psi & -\sin\psi \\ \sin\psi & \cos\psi \end{bmatrix} \begin{bmatrix} \cos\chi \\ j \sin\chi \end{bmatrix} \quad (11)$$

where α is an absolute phase term, ψ is the orientation angle of the polarization ellipse and χ the ellipticity angle of the polarization ellipse, as previously explained.

Table 1 shows the relation of the Jones vector and the parameters of the polarization ellipse for some polarization states.

Polarization state	Unit Jones Vector $\hat{\mathbf{u}}_{(x,y)}$	Orientation angle ψ	Ellipticity angle χ
Linear polarized in the x-direction: Horizontal (H)	$\hat{\mathbf{u}}_H = \begin{bmatrix} 1 \\ 0 \end{bmatrix}$	0	0
Linear polarized in the y-direction: Vertical (V)	$\hat{\mathbf{u}}_V = \begin{bmatrix} 0 \\ 1 \end{bmatrix}$	$\frac{\pi}{2}$	0
Right hand circular polarized (RCP)	$\hat{\mathbf{u}}_R = \frac{1}{\sqrt{2}} \begin{bmatrix} 1 \\ -j \end{bmatrix}$	$\left[-\frac{\pi}{2} \dots \frac{\pi}{2} \right]$	$-\frac{\pi}{4}$
Left hand circular polarized (LCP)	$\hat{\mathbf{u}}_L = \frac{1}{\sqrt{2}} \begin{bmatrix} 1 \\ j \end{bmatrix}$	$\left[-\frac{\pi}{2} \dots \frac{\pi}{2} \right]$	$\frac{\pi}{4}$

Table 1. Jones vectors and the corresponding polarization ellipse parameters for some canonical polarization states

3.4 Scattering or Sinclair matrix

Given the Jones vectors of the incident and the scattered waves, \underline{E}_I and \underline{E}_S , respectively, the scattering process at the target can be represented in terms of these Jones vectors as (12) [6]

$$\underline{E}_S = \frac{e^{-jkr}}{r} S \underline{E}_I \quad (12)$$

where k is the wavenumber and matrix S is the complex 2×2 *scattering* or *Sinclair matrix*. The term $\frac{e^{-jkr}}{r}$ takes into account the propagation effects both in amplitude and phase. In a fully polarimetric case, a set of four complex images is available. The scattering matrix S represents each pixel in the set and is given by (13)

$$S = \begin{bmatrix} S_{HH} & S_{HV} \\ S_{VH} & S_{VV} \end{bmatrix} \quad (13)$$

where its four elements S_{ij} are referred to as the *complex scattering coefficients*. The diagonal elements of the scattering matrix, S_{HH} and S_{VV} , are called *copolar* elements, since they relate the same polarization for the incident and the scattered fields. The orthogonal to the diagonal

elements, S_{HV} and S_{VH} , are known as *cross-polar* elements since they relate orthogonal polarization states. In monostatic radars, the reciprocity property holds for most targets, so $S_{HV} = S_{VH}$, i.e. the scattering matrix is symmetrical and has only 3 independent elements. Equations 12 and 13 are valid only in the far-field zone where the incident and scattered fields are assumed to be planar.

Different scattering vectors are defined depending on polarization basis. The complex Pauli spin matrix basis set $\{\psi_{4P}\}$ is widely used and is given by (14) [29].

$$\{\psi_{4P}\} = \left\{ \sqrt{2} \begin{bmatrix} 1 & 0 \\ 0 & 1 \end{bmatrix}, \quad \sqrt{2} \begin{bmatrix} 1 & 0 \\ 0 & -1 \end{bmatrix}, \quad \sqrt{2} \begin{bmatrix} 0 & 1 \\ 1 & 0 \end{bmatrix}, \quad \sqrt{2} \begin{bmatrix} 0 & -j \\ j & 0 \end{bmatrix} \right\} \quad (14)$$

The coefficient $\sqrt{2}$ is used to normalize the corresponding scattering vector \underline{k} and to keep the total power invariant, that is $\|\underline{k}\|^2 = \text{Span}(S)$. The scattering vector or covariance vector \underline{k} is a vectorized version of the scattering matrix and is required in order to extract the physical information about the target. For bistatic scattering case, the 4-D \underline{k} -target vector or 4-D Pauli feature vector is given by (15).

$$\underline{k}_4 = \frac{1}{\sqrt{2}} [S_{HH} + S_{VV}, S_{HH} - S_{VV}, S_{HV} + S_{VH}, j(S_{HV} - S_{VH})]^T \quad (15)$$

The scattering matrix S is thus related to the polarimetric scattering target vectors as (16).

$$S = \begin{bmatrix} S_{HH} & S_{HV} \\ S_{VH} & S_{VV} \end{bmatrix} = \frac{1}{\sqrt{2}} \begin{bmatrix} k_1 + k_2 & k_3 - jk_4 \\ k_3 + jk_4 & k_1 - k_2 \end{bmatrix} \quad (16)$$

For monostatic radar case, the 4-D polarimetric target vector reduces to 3-D polarimetric target vector. In this case, the complex Pauli spin matrix basis set $\{\psi_{4P}\}$ results in (17) [30].

$$\{\psi_{3P}\} = \left\{ \sqrt{2} \begin{bmatrix} 1 & 0 \\ 0 & 1 \end{bmatrix}, \quad \sqrt{2} \begin{bmatrix} 1 & 0 \\ 0 & -1 \end{bmatrix}, \quad \sqrt{2} \begin{bmatrix} 0 & 1 \\ 1 & 0 \end{bmatrix} \right\} \quad (17)$$

The 3-D \underline{k} -target vector or 3-D Pauli feature vector is then given by (18).

$$\underline{k}_3 = \frac{1}{\sqrt{2}} [S_{HH} + S_{VV}, S_{HH} - S_{VV}, 2S_{HV}]^T \quad (18)$$

The elements of the 3-D Pauli feature vector, $S_{HH} + S_{VV}$, $S_{HH} - S_{VV}$ and $2S_{HV}$, represent odd reflection, even reflection and multiple reflection respectively [31].

3.5 Coherency matrix

In most geoscience radar applications, the scatterers are generally embedded in a dynamic environment, so they are affected by spatial and/or time variations. These scatterers, called partial scatterers or distributed targets, can no longer be completely described by a scattering matrix S [6]. The concept of coherency matrix was introduced to advance the analysis of partial scatterers in the complex domain [30].

For a reciprocal target matrix, in the monostatic backscattering case, the reciprocity constrains the Sinclair scattering matrix to be symmetrical, so $S_{HV} = S_{VH}$, thus, the 4-D polarimetric coherency $[T_4]$ matrix reduces to 3-D polarimetric coherency matrix $[T_3]$. The 3×3 coherency matrix $[T_3]$ is formed from the outer product of the Pauli scattering vector \underline{k}_3 , as (19) [6] [30].

$$[T_3] = \langle \underline{k}_3 \cdot \underline{k}_3^{*T} \rangle = \left\langle \begin{bmatrix} |k_1|^2 & k_1 k_2^* & k_1 k_3^* \\ k_2 k_1^* & |k_2|^2 & k_2 k_3^* \\ k_3 k_1^* & k_3 k_2^* & |k_3|^2 \end{bmatrix} \right\rangle \quad (19)$$

$$= \frac{1}{2} \begin{bmatrix} \langle |S_{HH} + S_{VV}|^2 \rangle & \langle (S_{HH} + S_{VV})(S_{HH} - S_{VV})^* \rangle & 2\langle (S_{HH} + S_{VV})S_{HV}^* \rangle \\ \langle (S_{HH} - S_{VV})(S_{HH} + S_{VV})^* \rangle & \langle |S_{HH} - S_{VV}|^2 \rangle & 2\langle (S_{HH} - S_{VV})S_{HV}^* \rangle \\ 2\langle S_{HV}(S_{HH} + S_{VV})^* \rangle & 2\langle S_{HV}(S_{HH} - S_{VV})^* \rangle & 4\langle |S_{HV}|^2 \rangle \end{bmatrix}$$

The coherency matrix $[T_3]$ is Hermitian positive semidefinite and contains all the physical information of each pixel.

For the dual-polarization case, each pixel is represented by a 2×2 coherency matrix $[T_2]$ that is obtained from $[T_3]$ by (20).

$$[T_2] = \langle \underline{k}_2 \cdot \underline{k}_2^{*T} \rangle = \left\langle \begin{bmatrix} |k_1|^2 & k_1 k_2^* \\ k_2 k_1^* & |k_2|^2 \end{bmatrix} \right\rangle \quad (20)$$

$$= \frac{1}{2} \begin{bmatrix} \langle |S_{HH} + S_{VV}|^2 \rangle & \langle (S_{HH} + S_{VV})(S_{HH} - S_{VV})^* \rangle \\ \langle (S_{HH} - S_{VV})(S_{HH} + S_{VV})^* \rangle & \langle |S_{HH} - S_{VV}|^2 \rangle \end{bmatrix}$$

Chapter 4

Indonesia Case Study description

4.1 TerraSAR-X spacecraft

TerraSAR-X is a German Earth observation satellite that was launched on June 15, 2007 in Baikonur (Kazakhstan) [32]. The partners of the missions are the German Aerospace Center (DLR), the German Federal Ministry of Education and Research and Astrium GmbH. The satellite is controlled from the DLR ground station in Weilheim. Since January 7, 2008, when the mission became fully operational, TerraSAR-X is providing value-added SAR data for scientific, commercial and research-and-development purposes [33].

TerraSAR-X acquires high-resolution and wide-area radar images independent of the weather conditions and presence/absence of sunlight. Its primary payload is an X-band radar sensor with a range of different modes of operation in the X-band [34], allowing it to record images with different swath widths, resolutions and polarizations.

The satellite has a Sun-synchronous circular repeat orbit with a repeat period of 11 days. The orbit has a pre-defined Earth-fixed reference orbit, which closes after a repeat cycle of 167 revolutions in 11 days (its time required to orbit the Earth is 94.85 minutes) [35].

Length	4.88 metres
Diameter	2.4 metres
Launch mass	1230 kilograms
Payload mass	About 400 kilograms

Radar frequency	9.65 Gigahertz
Power consumption	800 watt on average
Orbital altitude	514 kilometres
Rocket	Dnepr 1
Inclination angle with respect to the equator	97.4 degrees
Operational life	At least 5 years an extended lifetime of that least another 5 years (beyond 2018) is expected by the operator DLR

Table 2. Main parameters of TerraSAR-X satellite

The different modes of operation are the Spotlight mode, in which an area of 10 kilometres long and 10 kilometres wide is recorded at a resolution of 1 to 2 metres; the Stripmap mode, which covers a 30-kilometre-wide strip at a resolution between 3 and 6 metres; and the ScanSAR mode, in which a 100-kilometre-wide strip is captured at a resolution of 16 metres [36]. Hence, the use of the sensor can be tailored to the need of the application.

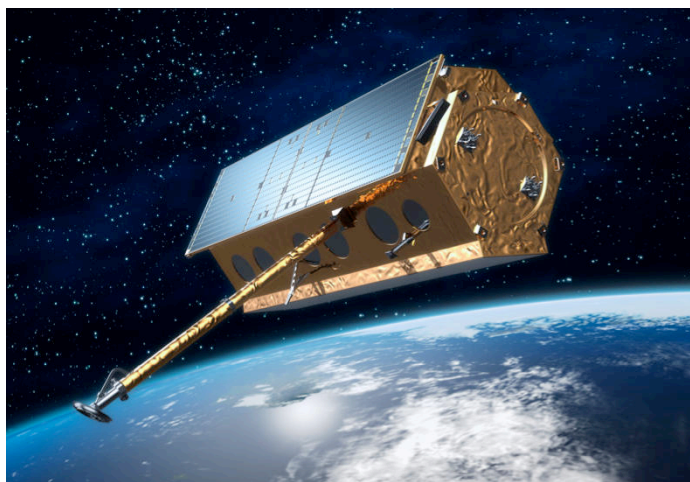


Fig. 10. Artist view of TerraSAR-X satellite

The antenna of TerraSAR-X is an electronically separable Active Phases Array Antenna with a size of 4.78 m x 0.7 m. During nominal operations, the SAR antenna is oriented with an angle of 33.8° degrees off the nadir direction looking right of the flight direction [37]. The antenna allows a variety of polarimetric combinations: single or dual-polarization and even full polarimetric data takes, are possible. Depending on the selected imaging mode there is available one combination or other.

Depending on the desired application, one of four different product types (processing levels) can be selected (Table 3) [37]. All the processing levels are available for the different modes of operation (StripMap, ScanSAR and SpotLight).

Processing Level	Contents
SSC (Single Look Slant Range Complex)	Single look product of the focused radar signal. The data are represented as complex numbers containing amplitude and phase information.
MGD (Multi Look Ground Range Detected)	Detected multi look product with reduced speckle and approximately square resolution cells.
GEC (Geocoded Ellipsoid Corrected)	Multi-look detected product, which is resampled and projected to the WGS84 reference ellipsoid assuming one average height.
EEC (Enhanced Ellipsoid Corrected)	Multi-look detected product, projected and resampled to the WGS84 reference ellipsoid and then corrected using an external Digital Elevation Model (DEM).

Table 3. Processing levels of TerraSAR-X satellite

4.2 TerraSAR-X delivery file format

The TerraSAR-X Basic Image Product is delivered in a standard set of components [38]. One of its components is the annotation information file, provided in xml format, which contains a complete description of the Level 1b product components and is considered as metadata source (provides information about the mission, the acquisition and the orbit, among others). The image channels contain one or more polarimetric channels in separate binary data matrices. These matrices are in the DLR-defined COSAR binary format when the data to deliver is complex and in GeoTiff format when the detected products are delivered.

The set also includes more files, like auxiliary raster files, quicklook images and map plots. The package is supplemented by additional administrative information, which describes the product delivery package and contains additional facility related information (e.g. detailed copyright information), and either archived into a *tar* file or put onto a medium.

4.3 Description of the Indonesia dataset

The dataset used in this thesis covers an area of Pangkalan Bun (Figure 11), a town in Central Kalimantan Province, Indonesia and was taken on 13th March, 2008. Its acquisition mode is TerraSAR-X StripMap and the processing level is SSC (Single Look Slant Range Complex), hence the image channel is in CoSAR format. It has dual-polarization mode and an incidence angle of 33.7°.

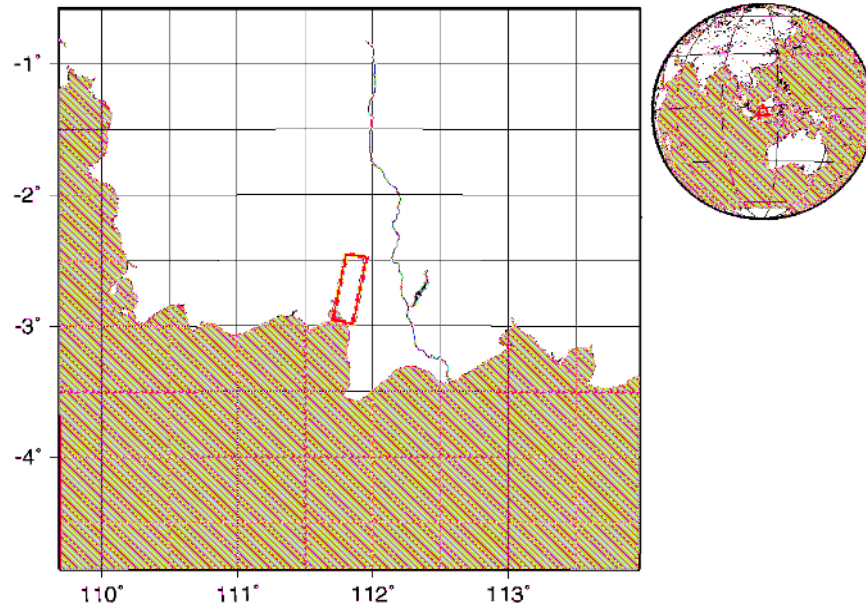


Fig. 11. Map of the area covered by the Case Study dataset

Some of the characteristics of the dataset are shown in Table 4.

Number of rows (ground range)	23361
Number of columns (azimuth)	10288
Image data format	CoSAR
Image data depth	32 meters
Polarization mode	HH-VV (dual-pol)
Ground range resolution	2.12 metres
Azimuth resolution	6 meters
Start time UTC	2008-03-13T22:19:55.140975
Stop time UTC	2008-03-13T22:20:03.140925

Table 4. Characteristics of the TerraSAR-X Indonesia dataset

Due to the large area that the SAR image covers and the high computational demand that this implies, three different subareas (Figure 12) of the main dataset are selected to carry out the

overall process of decomposition and segmentation. Working with different subareas also allows checking that the obtained results of the segmentation algorithm are independent of the input data. The selected subareas have some interesting zones for the posterior segmentation, like water, different types of vegetation and ships.

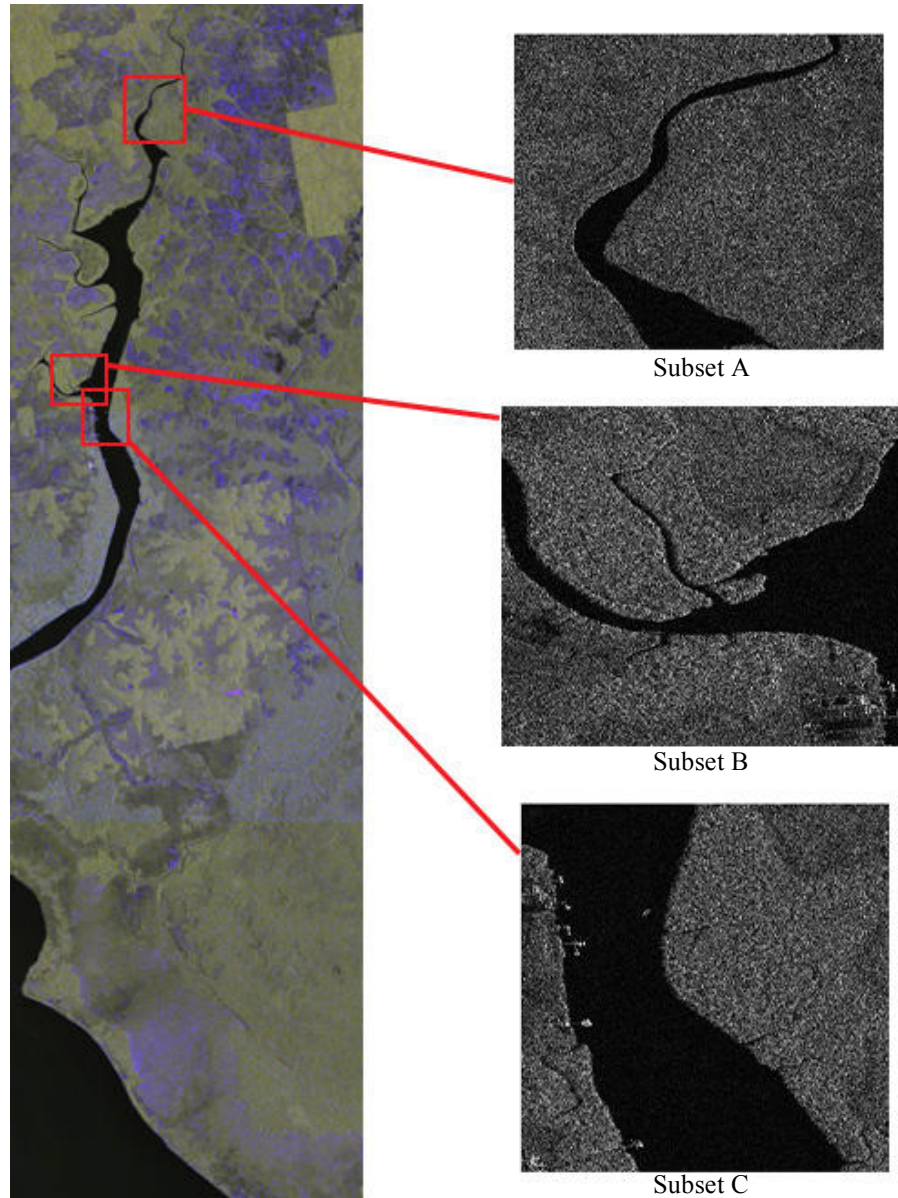
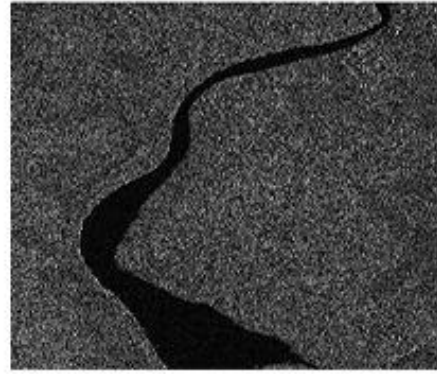
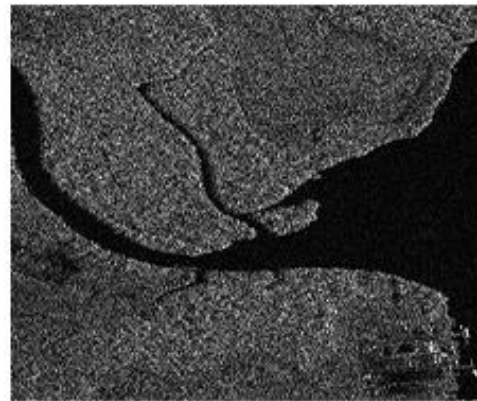


Fig. 12. Reconstruction image of the entire dataset and HH channels of the three selected subsets

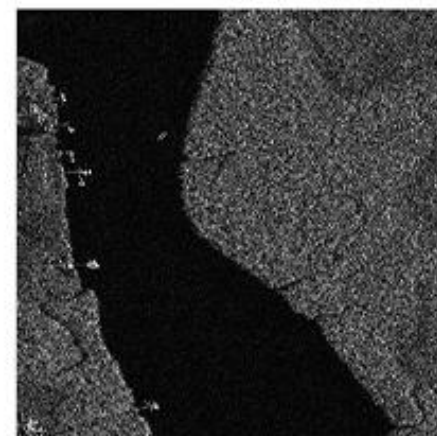
Figure 13 shows in detail the three subsets chosen for the analysis and segmentation, relating its HH channel matrix image with an aerial image of the same area captured by Google Earth. Note that the quality of Google Earth image in subset C is quite poor, fact that difficults the identification of each target. Also note that the HH-channel image seems a little deformed since its resolution in azimuth and in range are not the same.



Subset A



Subset B



Subset C

Fig. 13. Aerial image of the three subsets captured by Google Earth and their corresponding HH channel matrix image.

Chapter 5

H- α Decomposition applied to the Case Study

5.1 Theory of H- α Decomposition

Polarimetric decompositions are techniques used to generate polarimetric discriminators that can be used for analysis, interpretation and classification of SAR data [39]. These techniques allow the information extraction of the scattering processes that involve a specified target. There are two types of polarimetric decompositions; one is coherent decomposition, which is based in the decomposition of the scattering matrix, while the other, called incoherent decomposition is based in the decomposition of the coherency or covariance matrices [40]. H- α decomposition is an incoherent decomposition that analyzes the power form (the coherency matrix in this case) of the scattering matrix.

H- α decomposition is an entropy based decomposition method for quad polarization data proposed by Cloude and Pottier on 1997 [30]. This method is based on the hypothesis that the polarization scattering characteristics can be represented by the space of the entropy and the averaged scattering angle α by means of the eigenvalue analysis of Hermitian matrices. The H- α decomposition does not rely on the assumption of a particular underlying statistical distribution and so is free from the physical constraints imposed by such multivariate models. This method has such good properties as rotation invariance, irrelevance to specific probability density distributions and the coverage of the whole scattering mechanism space.

In this thesis dual-polarization (HH and VV) SAR data is used, so the H- α decomposition method has been extended in order to be applied to this data type.

5.1.1 Extraction of the H- α parameters

For the extraction of the entropy (H) and the alpha (α) parameters the coherency matrix explained in the Chapter 4 is needed. Remember that each pixel of the dual-polarization SAR data represents a 2 x 2 coherency matrix $[T_2]$, which is nonnegative, definite and Hermitian.

$$[T_2] = \begin{bmatrix} T_{11} & T_{12} \\ T_{21} & T_{22} \end{bmatrix} = \begin{bmatrix} T_{11} & T_{12} \\ T_{12}^* & T_{22} \end{bmatrix} \quad (21)$$

As mentioned previously, the H- α decomposition is computed by means of the eigenvalue analysis, so in (22), (23) and (24) the eigenvalue decomposition of the coherency matrix is done [30].

$$[T_2] = \begin{bmatrix} T_{11} & T_{12} \\ T_{21} & T_{22} \end{bmatrix} = U \begin{bmatrix} \lambda_1 & \\ & \lambda_2 \end{bmatrix} U^H = \lambda_1 u_1 u_1^H + \lambda_2 u_2 u_2^H \quad (22)$$

$$U = \begin{bmatrix} u_{11} & u_{12} \\ u_{21} & u_{22} \end{bmatrix} = [u_1 \quad u_2] \quad (23)$$

$$u_i = e^{j\phi_i} [\cos \alpha_i \quad \sin \alpha_i e^{j\delta_i}]^T \quad (24)$$

The subscript H denotes the Hermitian matrix, which is the conjugate transpose, so U^H is equivalent to U^{*T} .

Once the eigenvalues λ_1 and λ_2 and the eigenvectors u_1 and u_2 of the coherency matrix have been obtained, it is possible to compute the entropy H (25), which defines the degree of statistical disorder of each distinct scatter type within the ensemble, and the alpha α (26), which is related directly to underlying average physical scattering mechanism and hence may be used to associate observables with physical properties of the medium [41].

$$H = \sum_{i=1}^2 -P_i \log_2 P_i \quad (25)$$

$$\alpha = \sum_{i=1}^2 P_i \cos^{-1}(|u_{1i}|) \quad (26)$$

where P_i (27) correspond to the pseudo-probabilities obtained from the eigenvalues λ_1 and λ_2 . Since the eigenvalues are rotational invariant, the entropy H and the alpha α are also roll-invariant parameters.

$$P_i = \frac{\lambda_i}{\sum_{j=1}^2 \lambda_j}, \quad i = 1, 2 \quad (27)$$

Computing the preceding equations for the whole coherency matrix results in the entropy and alpha matrices, which have the half size of the coherency matrix due to for each group of 2x2 pixels in the coherency matrix, one value of entropy and one value of alpha are obtained. The entropy values are between 0 and 1, where a high value involves higher entropy in the pixel in question. The values of the alpha are between 0 and 90 degrees.

5.1.2 Interpretation of H- α feature space

The H- α plane is divided into nine basic regions characteristic of different scattering behavior, as shown in Figure 14 [30]. The basic scattering mechanism of each pixel of a polarimetric SAR image can be identified by comparing its entropy and α parameters to fixed thresholds. The location of the boundaries of the regions is set based on the general properties of the scattering mechanisms, but they can be modified to fit a particular dataset.

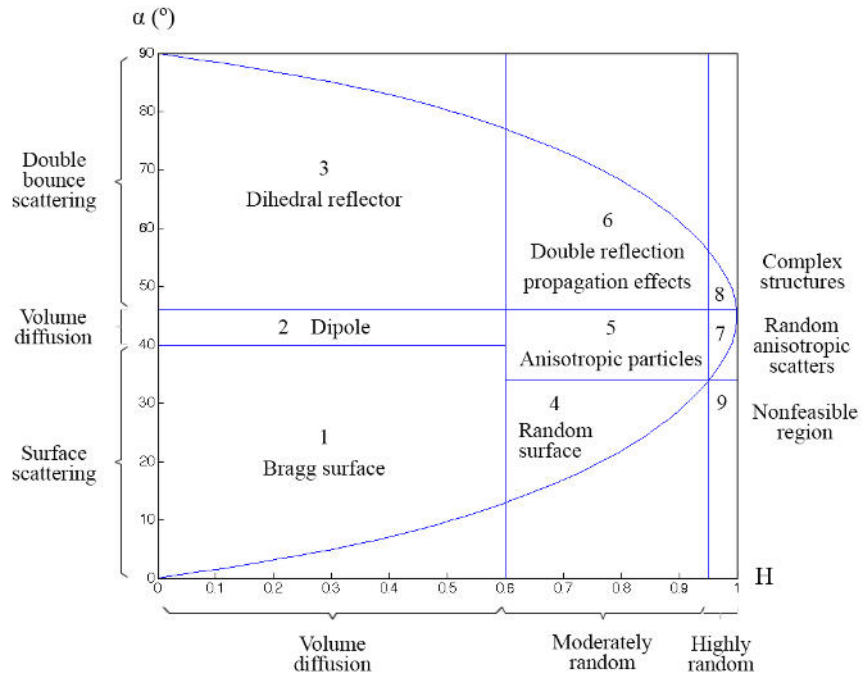


Fig. 14. H- α classification plane

Table 5 shows the typical scattering mechanism of each of the nine zones of the H- α feature space as well as its boundaries. Each zone is represented with a different color that will be useful for the results representation in Chapter 5.3.










Zone	Color	Scattering mechanism	Boundaries
1		Low entropy surface scattering	$\text{Alpha} \leq 40$ and $H \leq 0.6$
2		Low entropy dipole scattering	$40 < \text{Alpha} \leq 46$ and $H \leq 0.6$
3		Low entropy multiple scattering	$\text{Alpha} > 46$ and $H \leq 0.6$
4		Medium entropy surface scattering	$\text{Alpha} \leq 34$ and $0.6 < H \leq 0.95$
5		Medium entropy vegetation scattering	$34 < \text{Alpha} < 46$ and $0.6 < H \leq 0.95$
6		Medium entropy multiple scattering	$\text{Alpha} \geq 46$ and $0.6 < H \leq 0.95$
7		High entropy vegetation scattering	$34 < \text{Alpha} < 46$ and $H > 0.95$
8		High entropy multiple scattering	$\text{Alpha} > 46$ and $H > 0.95$
9		High entropy surface scattering (nonfeasible)	$\text{Alpha} \leq 34$ and $H > 0.95$

Table 5. Zones of H- α feature space

The different boundaries in the H- α plane discriminate between surface reflection, volume diffusion and double bounce reflection along the α axis and low, medium and high degree of randomness along the entropy axis [30]. Surface scattering is characteristic for agriculture fields, bare soils, flat surfaces and calm water, volume diffusion appears mainly over forested areas and double bounce scattering is typical for urban areas and buildings.

The alpha angle varies between 0° and 90° and allows the identification of the type of scattering process. If $\alpha = 0^\circ$, the scattering is related to plane surface, whereas for $\alpha = 45^\circ$, the result shows the scattering characteristics are those of a dipole. Between $\alpha = 0^\circ$ and $\alpha = 45^\circ$, it results in an irregular surface and for $\alpha = 45^\circ$ to $\alpha = 90^\circ$ the response is the result of a double bounce scatterer.

Lower values for entropy means that it is easier to extract information from the scattering. A higher value for entropy indicates that there are more than one scattering mechanisms and that they are equal in strength [42]. So, there is an increasing disability to differentiate scattering mechanisms as the entropy increases. If the entropy is close to zero, the alpha angle gives the

dominant scattering mechanism for that resolution cell i.e., scattering is volume, surface or double bounce. Entropy increases as a natural measure of the inherent reversibility of the backscatter data; hence it can be used for identification of underlying scattering mechanism.

5.2 Application of H- α Decomposition to the Case Study

The data flow diagram for the work carried in Matlab out using the Indonesia dataset is illustrated in Figure 15.

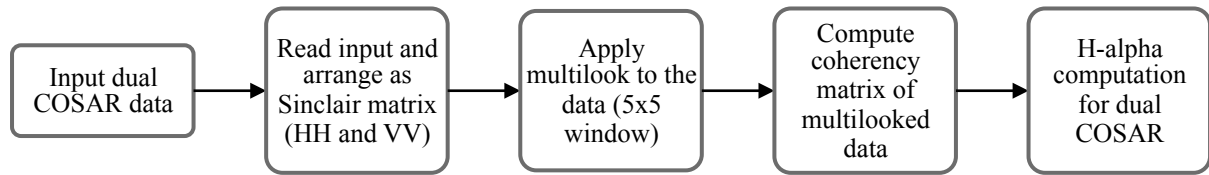


Fig. 15. Overall data flow diagram for the Case Study

The data flow has been applied to the three subsets of the Indonesia dataset and the results are shown in the Chapter 5.3.

5.3 Decomposition results of the Case Study

According to the flow diagram of Figure 15, the input dual-polarized COSAR Indonesia dataset has been read to extract separately the HH-channel and VV-channel matrices (Figure 16). Although the process has been applied to the three subsets of the Indonesia dataset, for the first steps it is shown only the subset A.

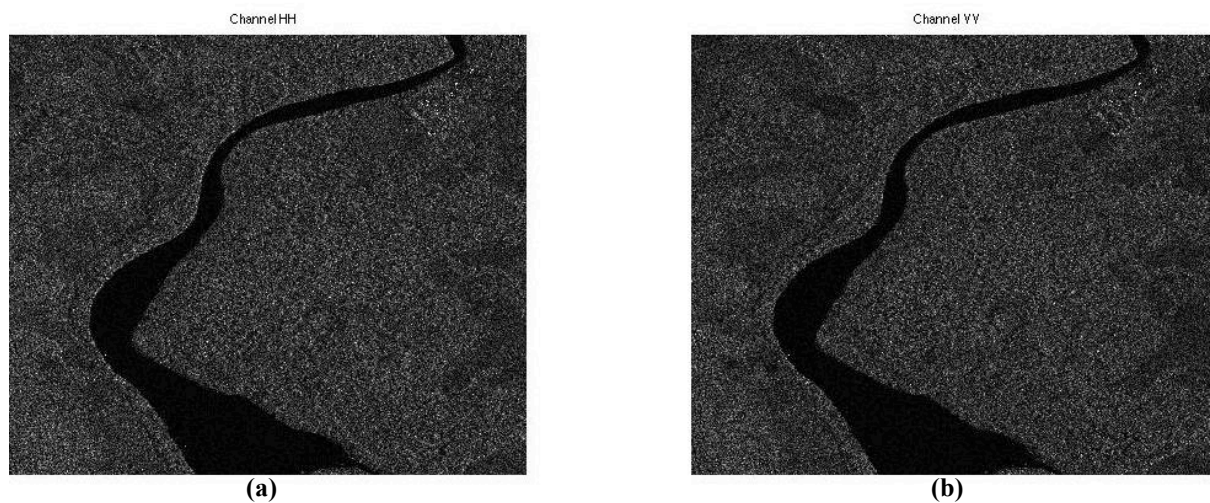


Fig. 16. Polarimetric channels of the subset A: (a) HH-channel, (b) VV-channel

The calm river water appears like a dark area in the SAR images since most of the incident radar pulses are specularly reflected away so very little energy is scattered back to the radar sensor. Forests and vegetation are usually moderately rough on the wavelength scale. Hence, they appear as moderately bright features in the SAR image. In the right-top corner of Figure 16 very bright targets appear, which indicates double-bounce effect where the radar pulse bounces off the horizontal ground towards the target and then the pulse is reflected from one vertical surface of the target back to the sensor. It happens because in this zone there are some buildings.

Once the HH-channel and VV-channel have been extracted, a square multilook window of five pixels has been applied in order to reduce the speckle noise that appears often in SAR images and create a more homogeneous image. The speckle noise is formed from coherent summation of the signals scattered from ground scatterers distributed randomly within each pixel.

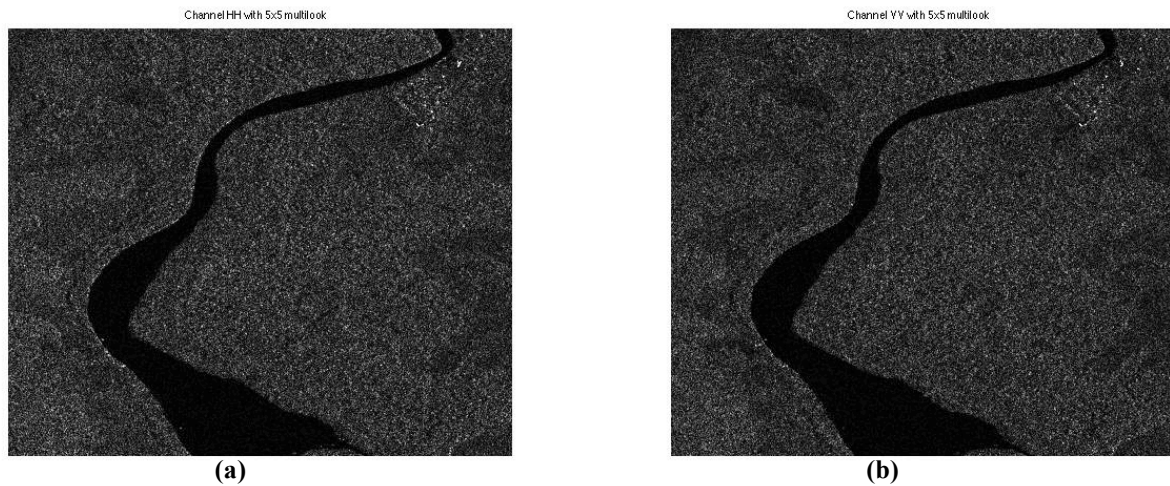


Fig. 17. Polarimetric channels of the subset A with 5x5 multilook window: (a) HH-channel, (b) VV-channel

After applying the speckle removal filter (Figure 17) there is not appreciated a substantial visual improvement in the image quality regarding the unfiltered input; however, for the computation of the coherency matrix this step is mandatory since it can considerably affect to the final results.

Once the multilooked HH-channel and VV-channel have been obtained, the coherency matrix, which will be fundamental for the H- α decomposition, is computed. With the obtained

coherency matrices (one for each subset), the H- α decomposition explained in 5.1 can be applied to the three different subsets of the Indonesia dataset.

- **Subset A**

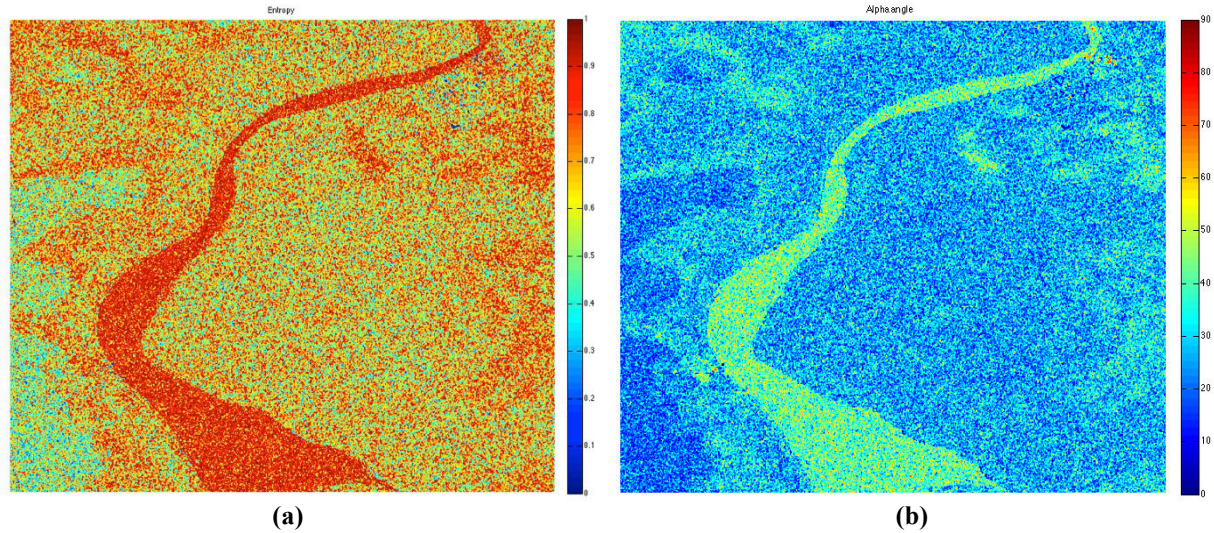


Fig. 18. Parameters extracted from the subset A: (a) entropy, (b) alpha angle

In Figure 18.a the entropy of the subset A is shown. The highest values of entropy appear in the river and in some areas of the forest (mainly located at the right of the image). For smooth river surfaces, with little or no relief at the scale of the radar wavelength, there is little return energy as the incident wave undergoes specular reflection. These areas are associated with high alpha and high entropy, indicating that very low amplitude backscatter is mainly random noise. Forest areas with high entropy appear since they are areas with more sparse vegetation and dryer than the rest of the forest. In areas of dry soil some of the incident radar energy is able to penetrate into the soil surface, resulting in less backscattered intensity. The rest of the forest, occupying the main part of the image, has medium entropy due to the increased density of vegetation in a uniform way. The zones with the lowest values of entropy appear in the left of the image where there are some crops. Those crops follow a more ordered and homogeneous structure than the forests, which entails in lower values of entropy.

In Figure 18.b the alpha angle of the subset A is shown. Medium-high alpha values appear in the river and some forests zones (the same areas that have the highest values of entropy) as a volume diffusion mode. The crops have the lowest alpha (with values lower than 30 degrees), which indicates surface scattering. In the top right of the image as well as in the bottom left, there are some very high alpha values due to in these zones there are some buildings with medium height (Figure 19.a and 19.b) that generates double bounce scattering, so the radar

beam bounces twice off the ground and the wall surfaces and most of the radar energy is reflected back to the radar sensor.

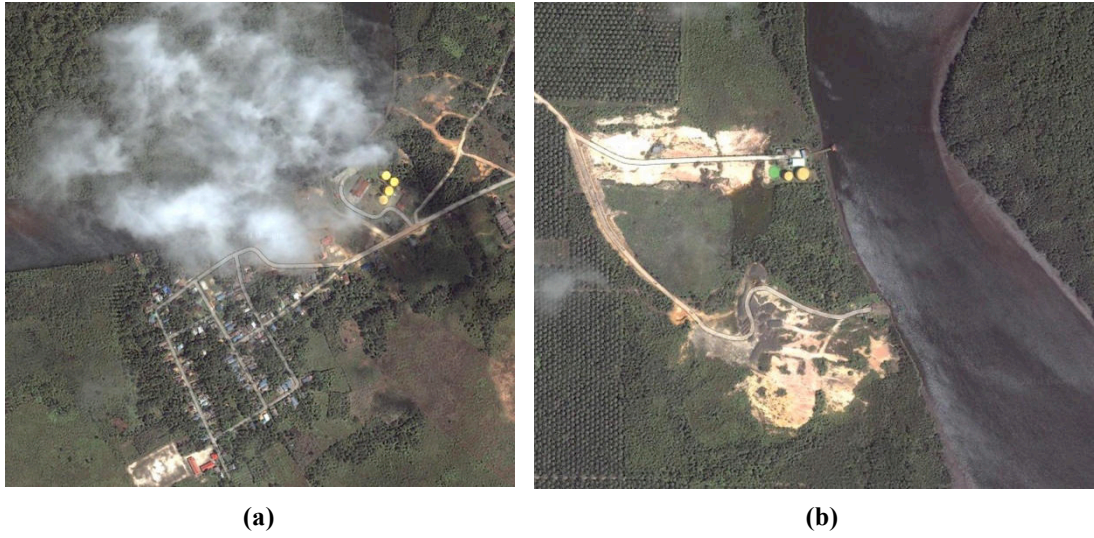


Fig. 19. Zoom of the zones with the highest alpha in subset A produced by the yellow buildings.

The corresponding H- α plane for the subset A is represented in Figure 20.

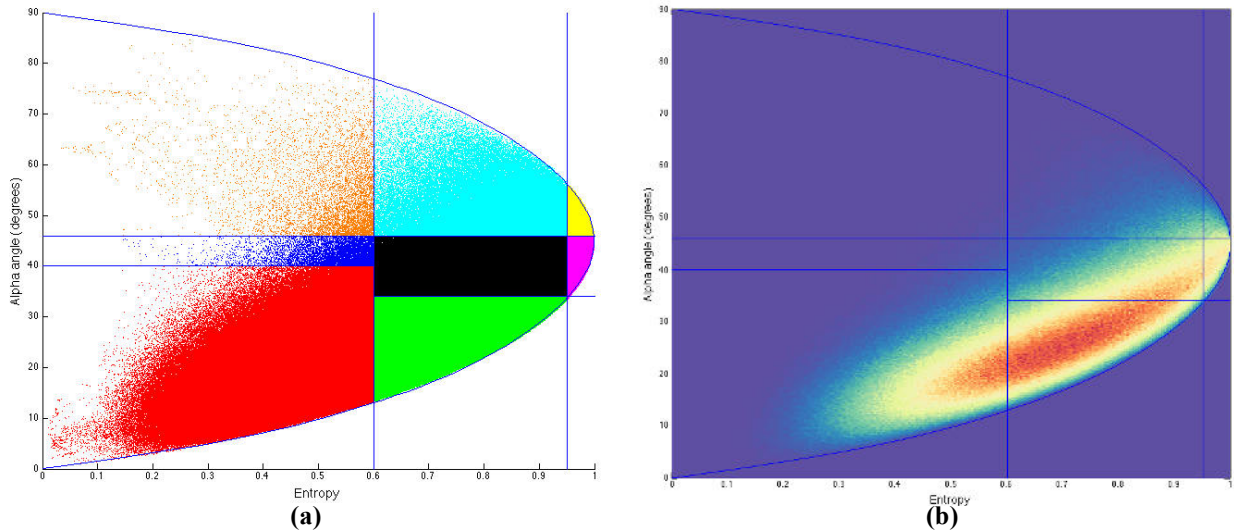


Fig. 20. H- α plane of the subset A: (a) zones with different colors, (b) density plot of the plane

Each of the nine zones of the H- α plane has been represented with their corresponding color according to Table 5 (Figure 20.a). This will allow doing a first classification of the subset depending on the zone to which each pixel belongs (Figure 21). A density plot for the H- α plane is shown in Figure 20.b since it is difficult to visually determine in which areas there is more density of pixels. The color of each point of the density plot represents the frequency of pixels within that region of the grid, which enables to visualize which are the more characteristic scattering mechanisms of the terrain.